

A MULTI-WAVELENGTH STUDY OF THE MIXED-MORPHOLOGY SUPERNOVA REMNANT W28

J. W. Keohane

Spitzer Science Center, JPL/Caltech

MS 220-06, 1200 California Blvd., Pasadena, CA 91125-0600, U.S.A.

KEOHANE@IPAC.CALTECH.EDU

J. Rho, T. G. Pannuti, K. Borkowski, P. F. Winkler

RHO@IPAC.CALTECH.EDU, TPANNUTI@IPAC.CALTECH.EDU, KBORKOW@UNITY.NCSU.EDU, WINKLER@MIDDLEBURY.EDU

Abstract

We present X-ray (*Chandra* and *ROSAT* HRI and narrow-band optical images of the mixed-morphology supernova remnant W28. We spatially compare these data with VLA maps that have been previously published in the literature.

The *ROSAT* HRI mosaicked image shows the well-known center-filled X-ray morphology, as well as a few sharp filamentary structures. Narrow-band optical images from the Curtis Schmidt telescope at Cerro Tololo International Observatory also reveal complex filamentary structure. There is a relative enhancement of [S II] compared to $H\alpha$ in the regions of known shock/cloud interactions and the converse is true in the central X-ray emitting region. Our *Chandra* image details the shape and extent of the central emission, revealing a bright knotty region approximately 5–10 arcminutes in size.

The *Chandra* data also reveal a hard X-ray point source coincident with the southwestern shell. This source is probably unrelated to W28, but it was responsible for the spectral variations previously observed by ASCA.

1 Introduction

Supernova remnants (SNRs) can be classified into four broad categories based on their radio and X-ray morphologies. The first class of SNRs feature shell-like radio and X-ray morphologies. The second class is Crab-like, with center-filled X-ray and radio non-thermal emission from an active pulsar. The third morphological category is a composite of the former two, with a well defined radio shell and central radio emission. Finally there are mixed-morphology SNR, which are

shell-like in their radio emission but are center-filled in thermal X-ray emission (Rho & Petre, 1998).

Mixed-morphology SNRs represent about 8% of the total SNR population and usually have nearly uniform temperature distributions (Rho et al., 1994; Rho & Petre, 1998). Almost all of these SNRs appear to be interacting with clouds, as indicated in some cases by strong infrared line emission or OH masers (Frail et al., 1996; Reach & Rho, 1996, 1998, 1999; Koo et al., 2001).

The supernova remnant W28 (G6.4–0.1) is the canonical mixed-morphology SNR (Rho & Petre, 1998; Rho et al., 2001). It has a relatively flat radio spectral index (Kassim, 1992; Dubner et al., 2000) and is known to be interacting with a dense molecular cloud (Wootten, 1981; Frail et al., 1993; Arikawa et al., 1999; Reach & Rho, 2000).

In this paper we present high-resolution X-ray and optical images. We compare these X-ray and optical images with each other as well as images of W28 that have been previously published in the literature.

2 Analysis

Table 1 lists our observational data sets, pointings and exposure times.

The *ROSAT* HRI images were exposure-corrected and mosaicked using the nine pointed observations shown in Table 1. The mosaicked image was created following the techniques of Snowden (1998), who kindly provided his software for our use. After producing a count-rate image with a pixel size of $12''$, we adaptively smoothed it using a smoothing kernel of 30 counts. It is this adaptively smoothed image which is

Table 1: Summary of observations of W28

Observatory & Instrument	Filter or Seq. Number	R.A. (h m s)	Decl. ($^{\circ}$ ' ")	Date	Exposure Time	Region of W28
<i>ROSAT</i> HRI	RH500382N00	18 00 48.0	-23 20 24.0	20 March 1995	24 ks	Center
<i>ROSAT</i> HRI	RH500382A01	18 00 48.0	-23 20 24.0	27 March 1996	11 ks	Center
<i>ROSAT</i> HRI	RH500484N00	18 01 19.2	-23 04 48.0	11 September 1998	27 ks	Northeast
<i>ROSAT</i> HRI	RH500485N00	17 59 14.4	-23 19 12.0	5 October 1997	15 ks	Northwest
<i>ROSAT</i> HRI	RH500486N00	18 01 43.2	-23 35 24.0	15 March 1998	4 ks	Southeast
<i>ROSAT</i> HRI	RH500486A01	18 01 43.2	-23 35 24.0	11 September 1998	15 ks	Southeast
<i>ROSAT</i> HRI	RH500487N00	18 00 19.2	-23 36 00.0	14 March 1998	14 ks	South
<i>ROSAT</i> HRI	RH500487A01	18 00 19.2	-23 36 00.0	8 September 1998	15 ks	South
<i>ROSAT</i> HRI	RH500488N00	17 59 00.0	-23 36 00.0	8 September 1998	7 ks	Southwest
<i>Chandra</i> ACIS	500278	18 00 24.6	-23 25 55.7	12 October 2002	87 ks	Center and SW
CTIO Curtis Schmidt	H α 6568/28	18 00 33	-23 25 00	22 June 1998	3 \times 600 s	All
CTIO Curtis Schmidt	[S II] 6738/50	18 00 33	-23 25 00	22 June 1998	3 \times 600 s	All
CTIO Curtis Schmidt	Red 6858/95	18 00 33	-23 25 00	22 June 1998	3 \times 300 s	All

shown in the figures.

The *Chandra* ACIS data were prepared from the raw event files (i.e., the `evt1` files) following the CIAO 3.0 data analysis threads. Images were extracted in three bands with soft, medium and hard energy ranges of 0.5–1.7 keV, 1.7–3.3 keV and 3.3–7.1 keV respectively. Each image was exposure corrected assuming monochrome emission in the middle of each bandpass. Next the CIAO task `CSMOOTH` was run on an image of the total counts, which generated a scale map. Next each of the three bands were smoothed using the scale length map that was generated from smoothing the map of total counts image.

The optical images listed in Table 1 were obtained from the 0.6m Curtis Schmidt telescope at CTIO, operating with a Tektronix 2048 \times 2048 CCD camera at the Newtonian focus. The scale is 2.3"/pixel, to give an overall field of 1.3 degrees, substantially larger than W28. Images were obtained through narrow-band interference filters with central wavelengths near the H α and [S II] $\lambda\lambda$ 6717, 6732 lines, plus a continuum band centered at 6858 Å. The latter was used to subtract most of the stellar emission and to reveal faint nebulosity.

3 Results and discussion

Figure 1 displays our *ROSAT* HRI mosaicked image, our H α image, and a VLA 330 MHz map kindly provided by G. Dubner (Dubner et al., 2000). Notice the large extent of the radio shell compared to either the X-ray or the optical emission. Also notice that the north-eastern shell is bright in both the X-ray and radio.

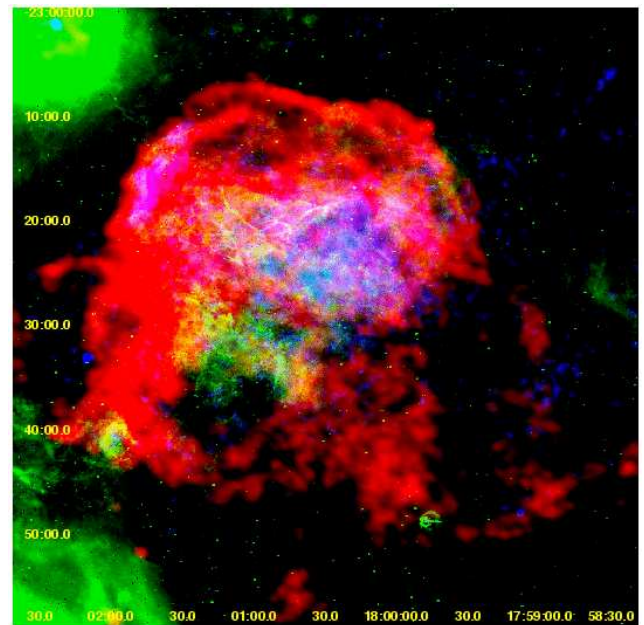


Figure 1: The λ 90 cm VLA map of Dubner et al. (2000) is shown in red. Our CTIO H α image is displayed in green, and our *ROSAT* HRI adaptively smoothed mosaic is shown in blue. All images are logarithmically scaled.

Figure 2 shows our CTIO H α and [S II] images, overlaid with our *ROSAT* HRI data. Notice how well correlated the H α and [S II] images are on small scales.

Figure 3 shows our optical and *ROSAT* images in grayscale, along with the ratio of our [S II] to H α images. Notice how clearly the central X-ray bright cavity is defined as deficient in [S II] relative to H α , while the surrounding shell is relatively bright in [S II].

Figure 4 shows the PSPC image of W28 of Rho &

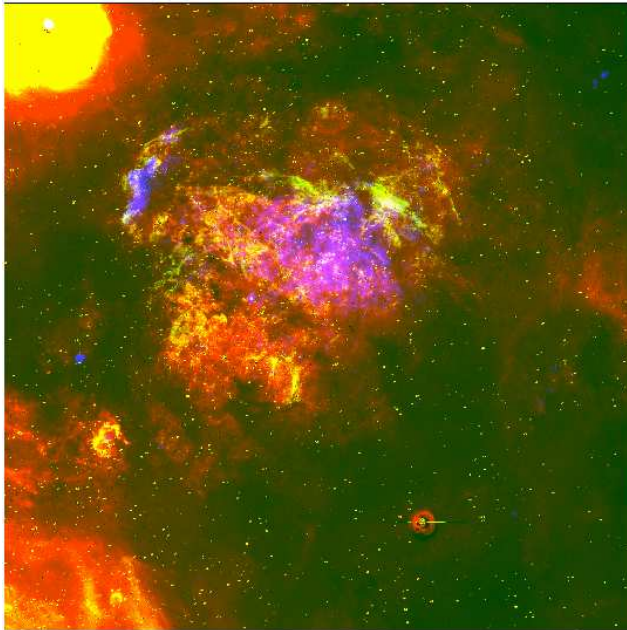


Figure 2: CTIO $H\alpha$ and [S II] images of W28 are shown in red and green respectively. The ROSAT HRI adaptively smoothed image is shown in blue. The burned out nebula in Northeastern corner is the Trifid nebula. Notice the enhanced [S II] emission surrounding the X-ray center. Images are linearly scaled.

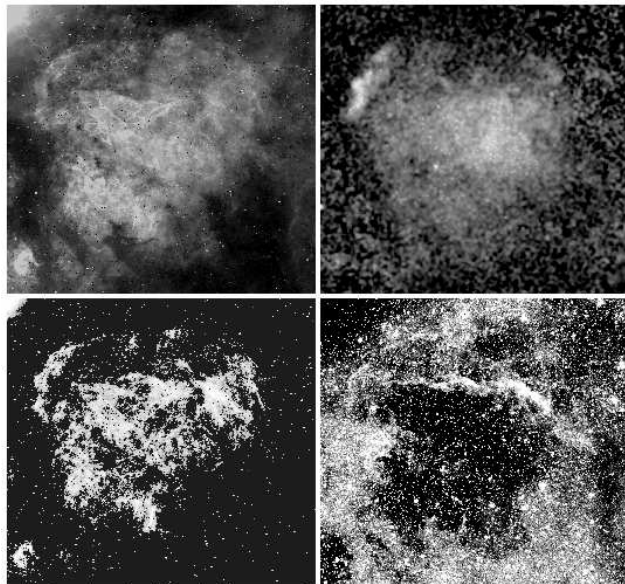


Figure 3: Counterclockwise from upper-right, the following images of W28 are shown: ROSAT HRI mosaic, CTIO $H\alpha$ image, CTIO [S II], and the ratio of [S II]/ $H\alpha$.

Borkowski (2002) with the *Chandra* hard contours overlaid. Figure 5 shows the unsmoothed true color *Chandra* image of all the chips. By simulating the

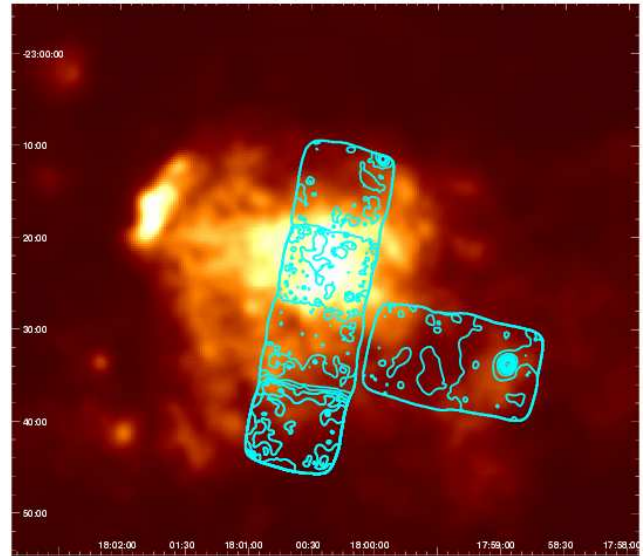


Figure 4: The ROSAT PSPC image (Rho & Borkowski, 2002) with contours of the hard *Chandra* emission overlaid.

Chandra point spread function on the I0 chip, we find that this hard source is consistent with its being point-like. The exact nature of this source is still uncertain but because its spectrum contains a strong iron line it is likely an object which contains an accretion disk, such as a background active galaxy. Nonetheless, it appears to be responsible for the harder southwestern emission as detected by ASCA (Rho & Borkowski, 2002). Excluding this source, the spectrum of the southwestern bar is not qualitatively different than the spectrum of the central region.

Figure 6 shows our smoothed and unsmoothed true color images of the central region. Notice the finite extent of the central region and the northwest-southeast direction of its elongation. Also notice the clumpy nature of the central region, with spatial variations in the X-ray color.

4 Conclusions

W28 is an observationally rich object, with detailed structures in each waveband. All of these structures appear to result from how the supernova shock is interacting, or has interacted, with the complex cloudy medium which surrounded its progenitor star. In addition to the spatial analysis presented here, a more detailed spectral study of the supernova remnant should be accomplished. Moreover, additional modeling of realistic stellar explosions inside complex molecular cloud structures are needed to interpret these data.

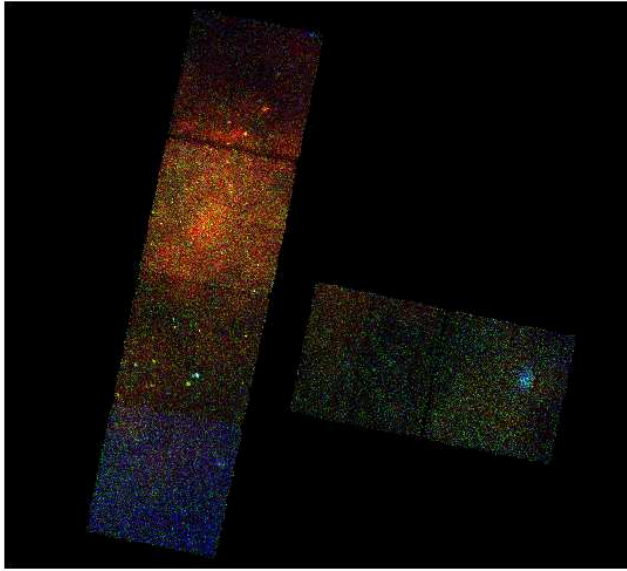


Figure 5: Unsmoothed, exposure corrected, true color image of the whole *Chandra* data set. The soft, medium and hard cuts are as follows: Red (0.5–1.7 keV), Green (1.7–3.3 keV) and Blue (3.3–7.1 keV).

Acknowledgments

We would like to thank G. Dubner for kindly providing us with the VLA data shown. We also thank W. Reach for helpful discussions. Support for this work was provided by NASA through *Chandra* grant NAS7-1407 and LTSA grant NRA-01-01-LTSA-013. PFW's optical work is supported by the NSF through grant AST-0307613

References

- Arikawa, Y., Tatematsu, K., Sekimoto, Y., Takahashi, T. 1999, PASJ, 51, L7
 Dubner, G. M., Velázquez, P. F., Goss, W. M., Holdaway, M. A. 2000, AJ, 120, 1933
 Frail, D. A., Kulkarni, S. R., Vasisht, G. 1993, Nature, 365, 136
 Frail, D. A., Goss, W. M., Reynoso, E. M., Giacani, E. B., Green, A. J., Otrupcek, R. 1996, AJ, 111, 1651
 Kassim, N. E. 1992, AJ, 103, 943
 Koo, B.-C., Rho, J., Reach, W. T., Jung, J., Mangum, J. G. 2001, ApJ, 552, 175
 Reach, W. T., Rho, J. 1996, A&A, 315, 277
 Reach, W. T., Rho, J. 1998, ApJ, 507, L93
 Reach, W. T., Rho, J. 1999, ApJ, 511, 836
 Reach, W. T., Rho, J. 2000, ApJ, 544, 843
 Rho, J.-H., Petre, R., Schlegel, E. M., Hester, J.J. 1994,

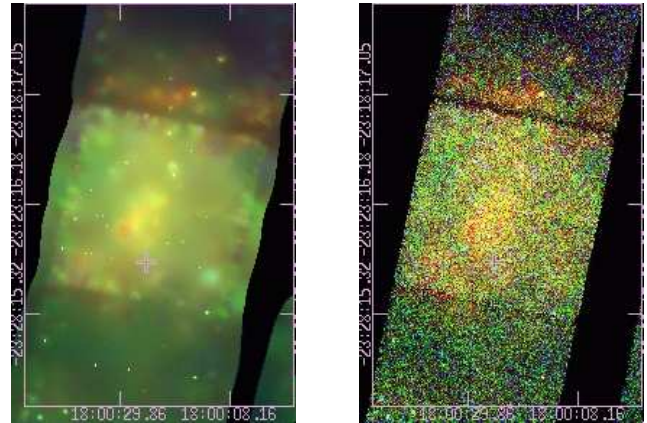


Figure 6: True color, exposure-corrected images of the X-ray bright central region of W28. The image on the left was adaptively smoothed using the CIAO CSMOOTH command, while the image on the right was not. The soft, medium and hard cuts are the same as Fig. 5. The purple cross denotes the location of the optical axis.

ApJ, 430, 757

Rho, J., Petre, R. 1998, ApJ, 503, L167

Rho, J., Jarrett, T. H., Cutri, R. M., Reach, W. T. 2001, ApJ, 547, 885

Rho, J., Borkowski, K. J. 2002, ApJ, 575, 201

Snowden, S. L. 1998, ApJS, 117, 233

Wootten, A. 1981, ApJ, 245, 105